Journal Pre-proof

A novel unknown-input and single-output approach to extract vibration patterns via a roving continuous random excitation

Zhuozheng Yang, Jun Pan, Jinglong Chen, Yanyang Zi,
Sebastian Oberst, C.W. Schwingshackl, Norbert Hoffmann
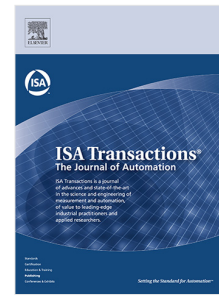
Please cite this article as: Z. Yang, J. Pan, J. Chen et al., A novel unknown-input and single-output approach to extract vibration patterns via a roving continuous random excitation. *ISA Transactions* (2021), doi: https://doi.org/10.1016/j.isatra.2021.12.011.

This is a PDF file of an article that has undergone enhancements after acceptance, such as the addition of a cover page and metadata, and formatting for readability, but it is not yet the definitive version of record. This version will undergo additional copyediting, typesetting and review before it is published in its final form, but we are providing this version to give early visibility of the article. Please note that, during the production process, errors may be discovered which could affect the content, and all legal disclaimers that apply to the journal pertain.

Title page showing Author Details

A novel unknown-input and single-output approach to extract vibration patterns via a roving continuous random excitation

Zhuozheng Yang[a], Jun Pan[a,b], Jinglong Chen[a,*,*], Yanyang Zi[a], Sebastian Oberst[b,c,d], C.W. Schwingshackl[b,*], Norbert Hoffmann[b]

[a]State Key Laboratory for Manufacturing and Systems Engineering, Xi'an Jiaotong University, Xi'an 710049, China
[b]Imperial College London, Mechanical Engineering, Exhibition Road, SW7 2AZ London, United Kingdom
[c] Centre for Audio, Acoustics and Vibration, University of Technology Sydney, Australia
[d] School of Engineering and IT, The University of New South Wales Canberra, Australia

Abstract

Operating deflection shape analysis allows investigating the dynamic behaviour of a structure during operation. It normally requires simultaneous, multi-point measurements to capture the response from an unknown excitation source (unknown-input and multiple-output), which can complicate its usage for structures without ease of access. A novel vibration pattern testing method is proposed based on a roving continuous random excitation employing a small robotic Hexbug device and a single-point measurement. The Hexbug introduces a random excitation in consecutive locations while roaming over the structure. The resulting multi-modal, time and location dependent response of the system is captured in a single location, and then analysed with a newly developed method based on empirical wavelet transform, multiscale morphological filtering and optimisation to extract the excited vibration patterns. The efficiency of the proposed method is experimentally demonstrated on a free-free and a cantilevered beam with comparison to mode shapes extracted by hammer test. The validation highlights its ability to extract several vibration patterns from a long slender structure with good accuracy and robustness, with the general ability to expand the usability of an operating deflecting shape analysis.

Keywords: Operating deflection shape analysis; empirical wavelet transform; multiscale morphological filter; random robotic excitation; Hexbug.

* Corresponding author.
E-mail address: jlstrive2008@163.com (J. Chen), *c.schwingshackl@imperial.ac.uk* (C.W. Schwingshackl)

Highlights:

1) It is proposed to use a small robotic device that roves around a structure to measure its Operating Deflection Shapes.

2) An advanced data post-processing routine based on the combination of Empirical Wavelet Transform and Multiscale Morphological Filtering is proposed.

3) Two different beam setups are tested to verity the effectiveness and repeatability of the proposed method.

4) The proposed method provides an alternative way to measure Operating Deflection Shape of long slender structures with a simple and cheap setup.

A novel unknown-input and single-output approach to extract vibration patterns via a roving continuous random excitation

Abstract

Operating deflection shape analysis allows investigating the dynamic behaviour of a structure during operation. It normally requires simultaneous, multi-point measurements to capture the response from an unknown excitation source (unknown-input and multiple-output), which can complicate its usage for structures without ease of access. A novel vibration pattern testing method is proposed based on a roving continuous random excitation employing a small robotic Hexbug device and a single-point measurement. The Hexbug introduces a random excitation in consecutive locations while roaming over the structure. The resulting multi-modal, time and location dependent response of the system is captured in a single location, and then analysed with a newly developed method based on empirical wavelet transform, multiscale morphological filtering and optimisation to extract the excited vibration patterns. The efficiency of the proposed method is experimentally demonstrated on a free-free and a cantilevered beam with comparison to mode shapes extracted by hammer test. The validation highlights its ability to extract several vibration patterns from a long slender structure with good accuracy and robustness, with the general ability to expand the usability of an operating deflecting shape analysis.

Keywords: Operating deflection shape analysis; empirical wavelet transform; multiscale morphological filter; random robotic excitation; Hexbug.

Nomenclature		r	principal coordinates
		rms_{l_1,l_2}	root mean square error between l_1 and l_2
Symbol	**Description**	s	position
AM-FM	Amplitude-Modulated and Frequency-Modulated	t	time
DIC	Digital Image Correlation	T	modal matrix
ESPI	Electronic Speckle Pattern Interferometry	$VP_{k,m}$	extracted k^{th} vibration pattern under SE size m

2

EWT	Empirical Wavelet Transform	$W_x(k,t)$	k^{th} wavelet coefficient function of signal x
LDV	Laser Doppler Vibrometers		
ODS	Operating Deflection Shape	$x(t)$	measured vibration signal
SE	Structure Element	$y_k(t)$	Hilbert transform of $\Delta f_k(t)$
SIMO	Single Input and Multiple Output	$z_{k,m}(t)$	absolute estimation of kth vibration pattern under SE size m
VP	Vibration Pattern		
UIMO	Unknown Input and Multiple Output	$\alpha_{k,m}$	a set of all local maxima in $z_{k,m}(t)$
UISO	Unknown Input and Single Output	$\beta_{k,m}$	a set of all local minima in $z_{k,m}(t)$
$A_k(t)$	envelope of $\Delta f_k(t)$	δ	sampling interval
$f_k(t)$	kth empirical mode	$\Delta A_k(t)$	amplitude difference of $A_k(t)$
F	excitation force	$\Delta f_k(t)$	amplitude difference of $f_k(t)$
$F_{CO,m}^{(\varepsilon)}$	multiscale close-open operator	η	estimation error at nodal lines
$F_{CO,m}^{(\bar\varepsilon)}$	averaged multiscale close-open operator	$\hat\phi_n(\omega)$.	wavelet function
g	structure element	$\hat\psi_n(\omega)$	scaling function
I_1, I_2	indexes for estimation improvement	ω_j	jth resonance frequency
l_1, l_2	Signals	$\{\omega_i\}$	a set of frequency boundaries
m	size of g	$E[\cdot]$	expectation
MS_k	kth mode shape function	$F^{-1}(\cdot)$	inverse Fourier transform
$n(t)$	random noise	$*$	convolution
$p_{k,m}(t)$	flipped estimation of kth VP under SE size m	$\oplus$	dilation
		Θ	erosion
pcc_{l_1,l_2}	Pearson's correlation coefficient between l_1 and l_2	$\circ$	opening
		$\bullet$	closing

3

1. Introduction

Structures such as pipes and beams are widely used in a variety of engineering applications, and their long, slender shape makes them prone to vibration problems. They can be easily tested in a laboratory environment via modal analysis, where excitation and measurement equipment can be easily placed. Normally this is tested with one known excitation and many other measured responses (SIMO approach). However, the modal analysis in the field, where pipework is often difficult to access due to its location or operating conditions, can be much more challenging [1].

Operating deflection shape (ODS) analysis has been developed to overcome some of these restrictions, where the vibration response of a system is obtained from an unknown forcing function (often generated by the machine itself), allowing to extract vibration patterns without an accurate knowledge of the excitation source. In general, mode shapes can be defined by interpreting or post-processing ODSs [2]. An ODS can be defined as any forced motion of two or more degrees of freedom of a structure [3]. An ODS test can be conducted employing an unknown-input and multiple-output (UIMO) approach, that is, no known excitation and simultaneous multi-point vibration measurements are applied [4]. This can lead to the requirement of many access points to a structure so that the magnitude and phase of enough locations can be obtained for a dynamic characteristic of the structure, which in turn can be used for the detection of damage [5,6] or finding weak supports [7,8] in the structure. The concept of ODS also allows combining the measurement or structural vibration under operating conditions with a validated finite element analysis to quickly identify detrimental excitation sources and design imperfections [9].

The need to measure in several locations for the extraction of an ODS has led to a focus on contactless measurement techniques including source localisation techniques, such as those based on expensive sensors including Laser Doppler Vibrometers (LDVs) [10-13], Digital Image Correlation (DIC) [14,15], acoustic holography [16-17] or Electronic Speckle Pattern Interferometry (ESPI) [18,19]. These methods have been widely used for full-field ODS or their approximations measurements and significant progress in the measurement and post-processing techniques has been achieved. However, one major drawback of these contactless approaches is the required line of sight to the structure of interest, which can somewhat limit their use in an industrial environment, where other components can get in the way. This has led to the development of some very specialized setups,

4

such as Collette et al. [20] approach to measuring torsional vibration of a railway wheelset with a rotational LDV, Schwingshackl et al. [21] constant scanning LDV technique for cylindrical structures or Olson et al. [22] four-camera DIC method to measure the displacement of optical targets on a rotor.

All these methods in common are the assumption that the unknown excitation source is in a fixed position, so that several, simultaneously obtained measurements can be used to extract the ODS. This minimizes the need for measurement locations on the system, making the approach potentially much more suitable for structures that are difficult to access.

To gain insight into the vibration behaviour of a difficult to access or excite structure, a novel unknown-input and single-output approach is proposed in this paper to extract structural vibration patterns in particular mode shapes which could then be used, among many applications, also for damage detection. The proposed technique picks up on the above idea of a roving excitation, relying on a single measurement point on a long, slender structure, a small robotic device as a roving exciter, and a newly developed analysis technique to post-process the data. The experimental setup for the measurement is introduced in Section 2 and the proposed novel data processing technique is described and demonstrate on a free-free beam in Section 3. The data quality and possible ways for refinement are examined in Section 4 before the introduced approach is validated on a cantilever beam set up in Section 5. The advantages and restrictions of the proposed method are discussed in Section 6 before conclusions in Section 7.

2. Experimental setup for VP measurement with roving continuous random excitation

The basic idea of the proposed approach to measures a VP of structures is the use of a small robotic device for excitation. The selected excitation system is a Hexbug Nano V2© toy robot from Innovation First Labs, Inc. in Fig. 1(a). It is a small battery-powered device that propels itself forward due to an interaction of its vibrating body and its inclined, flexible legs. It has an overall small size of $45\times15\times20$mm and weighs 7 grams only, minimizing the mass loading effect on the structure. A small electric motor with an out of balance mass generates the required forcing, which depending on the battery power, occurs between 60 and 120 Hz. When moving around, the robot's eight legs hit the ground constantly, generate a series of impulses in a nearly random manner. These impulses propel the robot forwards, where the traveling speed stays nearly constant, but the direction of travel seems

5

rather random and mainly depends on the boundary conditions (e.g., surface conditions, walls to hit…). This excitation allows to measure in locations that may otherwise be difficult to access, and also removes the need for an excitation source in the system, since not all systems will generate forcing during operation (e.g., pipework, supporting frames, …). This method is based on a single, vertically (z-direction) measuring acceleration sensor (Fig. 2a). The sensor is placed in the middle section of a beam's end, and the vibration generated by the small robot is used as the excitation (Fig. 2a). While the robot is moving across the structure, its "legs" will hit the structure repeatedly, leading to a random continuous impact excitation. Due to the law of reciprocity, a single sensor can then be used in combination with the continuously varying excitation location to pick up the modulation of the time history by the vibration patterns of the structure (similar to a roving hammer test).

Due to the small impact excitation produced by the robot, it is difficult to produce a vibration response in complex and heavy structures such as bridges. Therefore, in bridges and other structures, larger vehicles are generally used to generate a strong enough impact excitation [23,24]. For practical application, a robot with a stable and a controllable forward direction speed could be selected, which will further eliminate the need to control the boundary conditions. Vertical slim bridge beam is a very extreme example, which is generally long and narrow structures such as pipes. Using a robot with an adsorption and a separate excitation system will allow the generation of suitable forcing signals.

The legs of the Hexbug device are made of rubber to give them the required flexibility for the forward propulsion but unfortunately, this leads to relatively small impulse amplitudes on the structure and in return not very large response amplitudes. To increase the amplitude of the impulses for a better response measurement and reduce the impulse width for the excitation of a larger frequency spectrum, small steel needle tips were glued to the legs, as shown in Fig. 1(b), increasing the response amplitudes by about 50%.
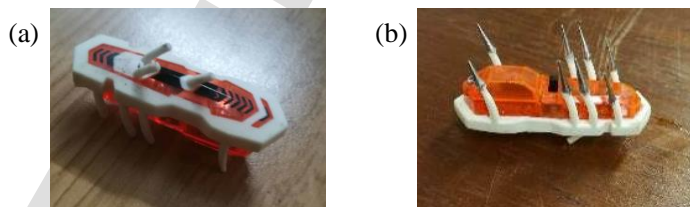
(a)   (b)

Fig. 1. (a) Hexbug Nano V2; (b) modified Hexbug Nano V2 (upside down) with steel feet.

6

This very simple excitation system was then applied to a free-free hanging C-section beam of 1,505 mm length (see Fig. 2) where the walls ensured that the robot would be guided along its length. A single accelerometer was attached near the entrance to measure the vertical vibration response and a small piece of paper was attached to the exit of the beam to reduce the transient of the robot falling off. A Data Physics Quattro DAQ system was used at a sampling frequency of 2,560 Hz to acquire the full traverse of the robot (~13 s).

An apparent problem was the rather random motion of the Hexbug, which not only caused forwards motion but also led to contestant bouncing between the sidewalls and sometimes temporary stuck conditions in a single location. This complicated the VP extraction significantly, since acquisition time and the robot location could not be linearly correlated. To overcome this issue a basic webcam was mounted above the open section of the C-beam (see Fig. 2) to observe the motion of the robot, and motion tracking in MATLAB was then used to link the actual excitation location to the recorded time series of the vibration response. A typical example of exciter position, *s(t)* over time, can be seen in Fig. 3(a). The position coordinate, *s*, is thereby defined from the exit of the beam towards the entrance, as shown in Fig. 2(b), meaning that the robot at t = 0 s is positioned at s = 1,505 mm on the beam, and it travels towards position s = 0 mm as time passes. Fig. 3(a) shows that in general the robot moves forward at a reasonable constant ratio, but the derived velocity of the robot in Fig. 3(b), indicates that the speed variation is actually quite large. Large roving speed variation will inevitably reduce the measurement accuracy. To ensure accurate measurements of the VP of the proposed system, motion tracking is introduced, which weakens the advantage of line-of-sight requirements, and also weakens the practicability of the proposed method. In future applications, more advanced actuators (such as actuators with follow-up cameras or actuators with high positioning accuracy) can be used to ensure a linear motion along a pipeline or a channel.
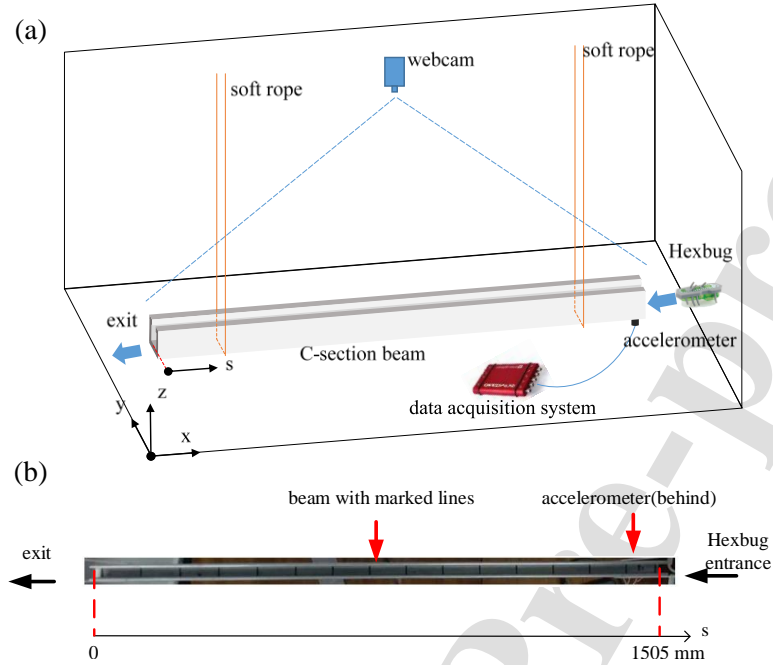
7

Fig. 2. (a) sketch of a hanged C-section free-free beam and (b) planform view of the beam with position coordinate.
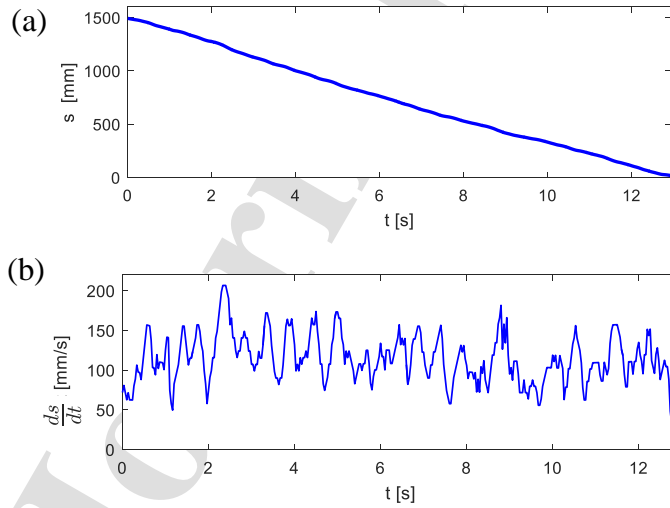

Fig. 3. (a) An example of time versus position relationship of Hexbug device, and (b) corresponding roving speed.

8

A roving hammer test was conducted on the free-free beam to identify its resonance frequencies and corresponding mode shapes, to obtain high-quality reference data. The beam was thereby hit centrally in the *z*-direction at the lines in Fig. 2(b), and the response was recorded with the single accelerometer of the setup. The data were analysed via the circle-fit method [1], leading to resonance frequency for the first three modes at 117 Hz, 316 Hz, and 573 Hz and the corresponding mass normalized bending mode shapes, MS_{1-3}, in Fig.4.
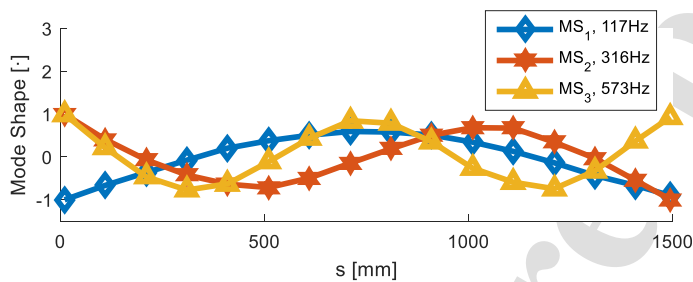

Fig. 4. Plot of the first three order mode shapes of the free-free beam. The amplitude is normalized.

A series of trials were then conducted with the robot, which was switched on and then carefully placed on the beam at the entrance located at $s = 1,505$ mm (see Fig. 2). As it ran along the beam the accelerometer data was recorded, leading to a typical time trace in Fig. 5(a). When the exciter is placed on the beam, there is an initial rapid increase in the multi-harmonic response signal, which then gets modulated by the mode shapes of the system as the robot travels along the beam. The final increase of the response signal at the exit of the beam (t ≈ 14 s) is caused by the effect of the exciter falling off the beam, after which the system response becomes a free decay. Fig. 5(b) shows the frequency spectrum of the recorded time history, indicating a series of resonance frequencies that match well with the impact hammer values. This highlights the ability of the Hexbug with the metal legs to excite frequencies above 1,000 Hz, which makes it usable for engineering structures.

Combining the time history data with the position data from the webcam leads to the plot in Fig. 5(c), which in principle corresponds to the sum of all the vibration patterns that are being excited by the randomly repeated impact excitation of the traveling robot. In the next step, a technique must be developed to accurately extract the VPs from the time history.
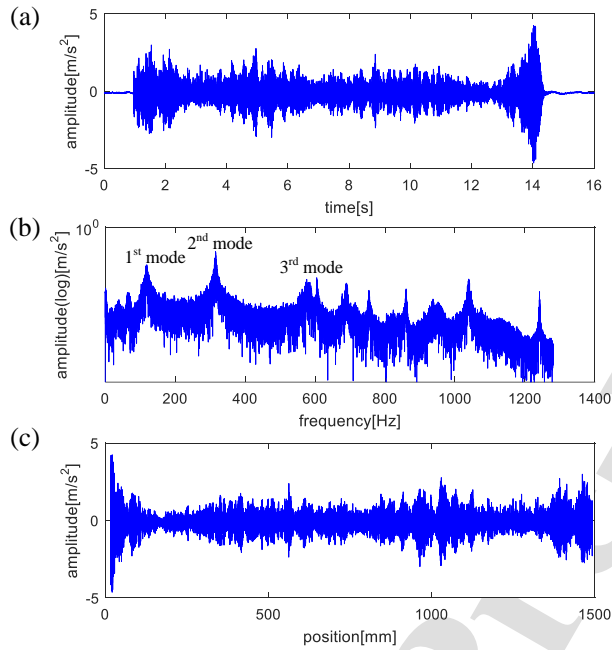
Fig. 5. Display of a testing signal from the free-free beam, (a) time waveform; (b) frequency spectrum, and (c) waveform amplitude versus position.

3. Data analysis technique for vibration pattern extraction with random roaming excitation

The analysis of the signals generated by the roving robot exciter in Fig. 5(c) is very challenging since the signal is a combination of several VPs that respond at the same time due to the more or less random nature of the traveling exciter. Traditional signal processing methods such as fast Fourier transform neither split the frequency band automatically nor extract VP from a complex time history. For this purpose, a novel approach is required, that can (i) separate the time history into its individual components, (ii) provide a reliable envelope of the shape, and (iii) allows to identify accurate VP.

3.1. Overview of basic background

A short overview of the relevant background will be presented here to facilitate the understanding of the introduced approach to analyse vibration data from random roving excitation. For more detailed information, the reader is referred to the quoted references.

10

3.1.1. Vibration analysis

To explain the rationality of the proposed data processing method theoretically, a reminder of the modal analysis shall be given. The equation of motion of an undamped linear multi-degree of freedom system is

$$\ddot{r}_j + \omega_j^2 r_j = T_j^T F(t),$$

(1)

where r_j are the principal coordinates, ω_j is j^{th} resonance frequency, T is the modal matrix where each column of T is a mode shape vector, and $F(t)$ is the excitation force [25]. Assuming a linear harmonic response, Eq. (1) has a solution for a given input force $F(t)$

$$r_j(t) = \frac{\dot{r}_j(0)}{\omega_j} sin\omega_j t + r_j(0) cos\omega_j t + \frac{1}{\omega_j} \int_0^t T_j^T F(t) sin\omega_j(t-\tau) d\tau,$$

(2)

where $r_j(0)$ and $\dot{r}_j(0)$ are the initial conditions. The solution in terms of the original variables can be then obtained [25] by

$$X(t) = Tr(t).$$

(3)

The derived solution of the equation of motion will be used in Section 3.2 to support the development of the proposed method.

3.1.2. Empirical Wavelet Transform

The Empirical Wavelet Transform (EWT) [26] is a time-frequency analysis method that allows to decompose a multi-harmonic time signal into its mono-components. The acquired signal is broken down into its mono-components by initially defining frequency boundaries $\{\omega_i\}$ that focus the analysis around each resonance frequency, for which the EWT method then constructs corresponding adaptive wavelets, $\phi_n(\omega)$ and $\psi_n(\omega)$. After the construction of adaptive wavelets, the approximation coefficients and detail coefficients of signal $x(t)$ can be computed by the inner products:

$$W_x(0,t) = \int x(\tau)\phi_n(\tau-t)d\tau = F^{-1}\left(\hat{X}(\omega)\overline{\hat{\phi}_n(\omega)}\right),$$

(4)

11

$$W_x(n,t) = \int x(\tau)\psi_n(\tau-t)d\tau = F^{-1}\left(\hat{X}(\omega)\overline{\hat{\psi}_n(\omega)}\right),$$ (5)

from which the mono-component f can be computed

$$f_0(t) = W_x(0,t) * \phi_1(t),$$ (6)

$$f_k(t) = W_x(k,t) * \psi_k(t),$$ (7)

to provide the decomposed original signal.

EWT allows to decompose the multi-harmonic signal from Fig. 5(a) into its mono-components f_k, which represents the vibration contributed from the kth mode only. A more detailed discussion about the EWT method for vibration analysis can be found in [27, 28].

3.1.3. Multiscale Morphological Filter

Morphological filtering [29] can be used to extract geometric features of the signal by adjusting four basic operators: dilation, $\oplus$, erosion, Θ, opening, $\circ$, and closing, $\bullet$, between the signal and a pre-defined structure element (SE), $g(m)$. Morphological filters provide a large range of possibilities to process data, where the main interest in this research lies on its ability to reduce noise and extract the global geometric shape of the signal via a close-open operator F_{CO}:

$$F_{CO,m} = (x \circ g \bullet g)(n),$$ (8)

which leads to the extraction of the "envelope" of a signal [30].

Building the operator F_{CO} requires the selection of an appropriate SE, g, where a flat SE shows good denoising ability [31]. The effectiveness of the F_{CO} is also greatly influenced by the size of the SE, $g(m)$. When it is too large some of the details in the signal are being lost while when it is too small results may be noisy. To help with the selection of the right parameters, a multiscale analysis [32] with a multi-dilated SE can be used

$$\varepsilon g(m) = \underbrace{(g \oplus g \oplus \cdots \oplus g)}_{\varepsilon-1 \, times}(m),$$ (9)

which builds up multiple SEs with different sizes based on the original $g(m)$. After defining the four basic multiscale operators based on Eq. (9), the multiscale close-open operator is defined as

11 / **31**

12

$$F_{CO,m}^{(\varepsilon)} = \left(x \circ \varepsilon g \bullet \varepsilon g \right)(n) \tag{10}$$

providing filtered "envelopes" of the signal x under different SE sizes. The final output of the multiscale filtering process with initial SE size m can then be obtained by averaging

$$F_{CO,m}^{(\bar{\varepsilon})} = \frac{1}{\lambda} \sum_{\varepsilon=1}^{\lambda} F_{CO,m}^{(\varepsilon)} \tag{11}$$

leading to an extracted "envelope" of the signal which less influenced by the initial choice of m, more details [32,33].

A combination of these shortly presented techniques will be used in the next section to develop an approach to extract the VP information from the roving exciter data from Fig. 5.

3.2. Absolute amplitude estimation of VP

Based on some of the theories presented in Section 3.1, in a first step the absolute amplitude estimation of the VP is required. The EWT is used to decompose the measured time signal $x(t)$ from Fig. 5(a) into its mono-components $f_k(t)$, which mainly contains vibration information from a single bending mode, k. Well separated resonance frequencies are required, so that the frequency boundaries can be manually determined from the frequency spectrum and no contamination from other resonances occurs.

If a mono-component is measured at time t_0 and at position s_0, which is denoted as $f_k(t_0)$ then from Eqs. (2) and (3), the amplitude difference of two consecutive measurements in time becomes

$$\begin{aligned}
\Delta f_k(t_0) &= f_k(t_0 + \delta) - f_k(t_0) = \ddot{X}_k(t_0 + \delta) - \ddot{X}_k(t_0) = T_k\left(\ddot{r}_k(t_0 + \delta) - \ddot{r}_k(t_0) \right) \\
&= T_k \omega_k \left(r_k(0) \omega_k \left(\cos\omega_k(t + \delta) - \cos\omega_k t \right) - \dot{r}_k(0)\left(\sin\omega_k(t + \delta) - \sin\omega_k t \right) \right), \\
&\quad + \frac{T_k}{\omega_k} \frac{d^2}{dt^2} \int_{t_0}^{t_0 + \delta} T_k^T F(t) \sin\omega_k(t - \tau) d\tau
\end{aligned} \tag{12}$$

where δ represents the sampling interval. If δ is small enough to consider $\omega_j \delta$ to be nearly zero, Eq. (12) can be simplified

$$\Delta f_k(t_0) \approx \frac{T_k}{\omega_k} \frac{d^2}{dt^2} \int_{t_0}^{t_0 + \delta} T_k^T F(t) \sin\omega_k(t - \tau) d\tau . \tag{13}$$

If the forcing function, $F(t)$, is known, then the VP can be estimated directly from Eq. (13). Unfortunately, in the presented approach, with a random roving exciter, the excitation force is unknown, requiring a different strategy to overcome the problem, so that then Eq. (13) becomes

$$\Delta f_k(t_0) \approx \frac{T_k}{\omega_k} n(t) e^{iw_k t} \Bigg|_{t=t_0}, \tag{14}$$

where $n(t)$ refers to a random noise signal. Eq. (14) implies that the envelope of $\Delta f_k(t)$ represents a multiplication of an unknown VP with a random noise signal. The VP can then be obtained by extracting the envelope of $\Delta f_k(t)$, for which originally the Hilbert transform [34] was used

$$y_k(t) = \frac{1}{\pi t} * \Delta f_k(t) = \int_{-\infty}^{+\infty} \frac{\Delta f_k(\tau)}{t-\tau} d\tau, \tag{15}$$

$$A_k(t) = \sqrt{\Delta f_k^2(t) + y_k^2(t)} \approx \left| \frac{T_k}{\omega_k} n(t) \right|, \tag{16}$$

where $A_k(t)$ is the envelope of each $\Delta f_k(t)$. Fig. 6(a) shows the envelope signal of the difference of the first mono-component, $A_1(t)$, for the free-free beam from Section 2. Although the envelope is quite noisy, the geometric shape of the absolute amplitude of the first bending mode is already visible, indicating that $A_k(t)$ is indeed a combination of the desired VP and random noise. The straightforward solution to extract the underlying VP would be to compute the expectation of $A_k(t)$, cf. Eq. (16)

$$E\big[A_k(t)\big] \approx E\left[\left| \frac{T_k}{\omega_k} n(t) \right| \right] \propto |T_k|, \tag{17}$$

which implies that $E\big[A_k(t)\big]$ is proportional to the absolute value of the mode shape vector. Given the requirement for an unlimited amount of data for the calculation of the expectation, this approach unfortunately is also not feasible.

Another way to estimate the VP is therefore needed, and it is proposed to use the MMF technique in Section 3.1.2 to extract the upper geometric shape of the $A_k(t)$

14

$$z_{k,m}(t) = F_{CO,m}^{(\bar{\varepsilon})}(A_k(t)). \tag{18}$$

Setting the correct filter parameters is not straightforward, but via trial and error an SE size m of 1,024 was initially found to be suitable. The filtered shape $z_{1,m}(t)$ of the envelope signal $A_1(t)$ from Fig. 6(a) is shown in Fig. 6(b). By comparing Fig. 6(b) to the mode shape data in Fig. 4, it can be seen that $z_{1,m}(t)$ looks somewhat similar to the absolute value of the 1st mode shape, making it a first approximation of the first VP of the structure.

The quality of the filtered shape $z_{k,m}(t)$ strongly depends on a series of parameters that have to be selected during the analysis: (i) the pre-defined frequency set $\{\omega_i\}$ for the EWT, needs to be selected accurately to ensures that each mono-component contains vibration from one mode only; (ii) the SE size m is impacting the quality of the extracted VP estimation, although MMF is used to reduce this influence; (iii) the approach to extract the shape $z_{k,m}(t)$ always provides absolute values and the MMF does not provide exact zeroes at the nodal lines. Improvements to the estimation of the filtered shape $z_{k,m}(t)$ are therefore required to provide VP with better quality.
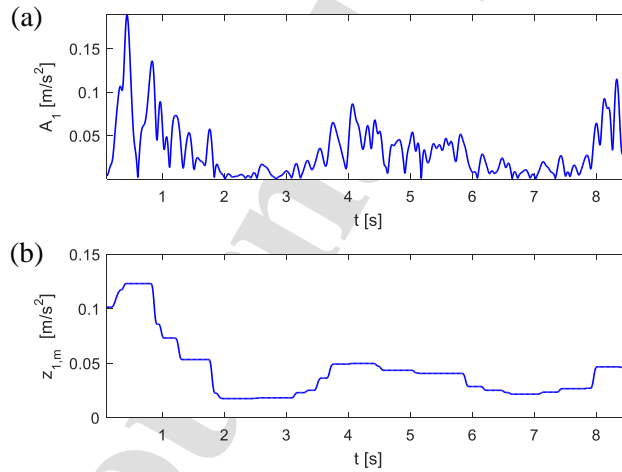

Fig. 6. (a) Display of the envelope signal, $A_1(t)$, and (b) multiscale morphological filtering result of $A_1(t)$.

3.3. Estimation improvement

A series of improvements to the proposed basic approach from Section 3.2 were introduced, to increase the accuracy of the estimated VP, $z_{k,m}(t)$.

3.3.1. Frequency boundary improvement

Initially the frequency boundary, $\{\omega_i\}$, for each mono-components in EWT was selected manually by trial and error. The effect of the frequency boundary $\{\omega_i\}$ for the first mode can be seen from Fig. 7(a) and (b), where different boundaries can lead to quite significant changes in the VP amplitudes.

To reduce this sensitivity of the VP extraction to the frequency boundaries, an approach is needed that determines how suitable the selected boundaries are. A good result should thereby be close to the corresponding mode shape from the hammer test, but since the exact mode shape will not be known a priory, a different quality index is needed.

What can be assumed is that the local maxima of $z_{k,m}(t)$ refer to peaks of the VP and the local minima of $z_{k,m}(t)$ indicate that the exciter is close to a nodal line of the mode shapes. Based on this assumption an index I_1 has been introduced which determines which frequency boundary $\{\omega_i\}$ setting provides the best separation of the local maxima and minima in the dataset

$$I_1 = \frac{\overline{\alpha}_{k,m} + \min(\alpha_{k,m})}{\overline{\beta}_{k,m} + \max(\beta_{k,m})}, \tag{19}$$

where $\alpha_{k,m}$ is the set of all local maxima in $z_{k,m}(t)$ and $\beta_{k,m}$ is the set of all local minima in $z_{k,m}(t)$. If a mode shape has no nodal lines, $\alpha_{k,m}$ or $\beta_{k,m}$ will be empty in which case a second index I_2

$$I_2 = \frac{\max\left(\left|\Delta z_{k,m}(t)\right|\right)}{\max\left(z_{k,m}(t)\right)} \tag{20}$$

can be used to describe the gradient change in the dataset. The assumption thereby is that a mode shape of a structure is a continuous smooth curve without significant gradient change, and the smaller the changes are between points, the less error is present in the VP shape.

16

Minimisation of I_1 or I_2, leads to an optimal set of the frequency boundaries, $\{\omega_i\}$, for the EWT. Searching the entire space of $\{\omega_i, \omega_{i+1}\}$ is very time-consuming and simple bilinear search is used instead: initially ω_{i+1} is fixed and the optimized lower boundary ω_i^* is found, After which ω_i^* is kept fixed and the optimal ω_{i+1}^* is found, leading to the optimised frequency boundaries $\{\omega_i^*, \omega_{i+1}^*\}$ for each mono-component extraction. This optimisation approach may not lead to the best result, but the found boundaries give satisfactory results.
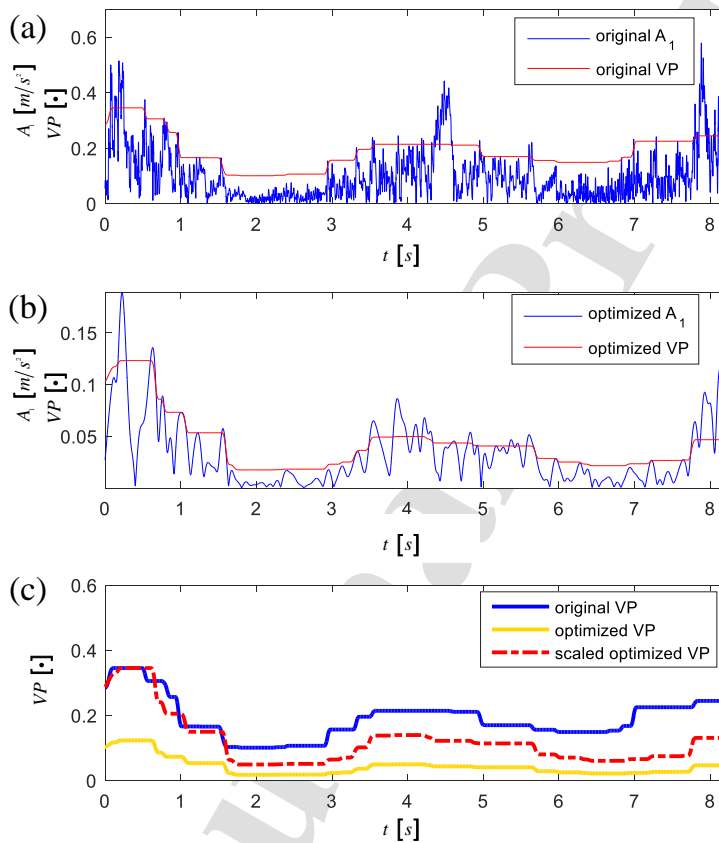

Fig. 7. (a)Extracted $A_1(t)$ (in blue) and $z_{1,m}(t)$ (in red) with initial boundaries [70 200], $I_1 = 1.76$; (b) Extracted $A_1(t)$ (in blue) and $z_{1,m}(t)$ (in red) with optimized boundaries [105 125], $I_1 = 2.91$, and (c) comparison of the two absolute VP results before and after optimization.

17

Fig. 7(c) shows a comparison of the extracted absolute VP estimations before and after the bilinear optimisation of the frequency boundaries for the first mode. The different frequency boundaries lead to different energy content in the extracted signal, leading to different amplitudes of the shapes. Since the main purpose of optimisation is to separate local maxima and minima, a scaled result after optimization is added to the plot with the same maximum amplitude as the one before optimization. From Fig. 7(c) the optimized result shows local minima which are closer to zero, leading to a better-defined absolute VP.

3.3.2. Flipping and scaling

Due to the absolute operator in Eq. (16), $z_{k,m}(t)$ is the absolute estimation of the VP shapes. The unknown excitation force from the robot prevents the extraction of the phase directly and a different approach will be needed.

Given that $z_{k,m}(t)$ is an absolute estimation of the VP, it can be assumed that its local minima represent nodal lines on the structure. Based on this, the signal after each local minimum can be mirrored around the position axis, leading to the flipped shape in Fig. 8, which is already a much better representation of the real VP. Due to the envelope estimation error near the nodal lines from the MMF technique, the repeated flipping, around these minima, introduces an artificial offset

$$\beta_{k,m}^*(i) = 2\beta_{k,m}(1) - \beta_{k,m}(i), \tag{21}$$

which must be subtracted from the processed signal, depending on the VP of the structure

$$\eta = \begin{cases} 2\beta_{k,m}(1) - \overline{\beta_{k,m}} & \text{if } \alpha_{k,m} \text{ is not empty} \\ \min(z_{k,m}(t)) & \text{if } \alpha \text{ is empty} \end{cases} . \tag{22}$$

The max-amplitude-scaled VP estimation versus time can then be obtained from the flipped shape $p_{k,m}(t)$ and its correction η by

$$VP_{k,m}(t) = \frac{p_{k,m}(t) - \eta}{\max\left(\left|p_{k,m}(t) - \eta\right|\right)}. \tag{23}$$

By substituting time, t, with position $s(t)$ in Eq. (23), the final $VP_{1,m}(s)$ can be obtained in Fig. 9.
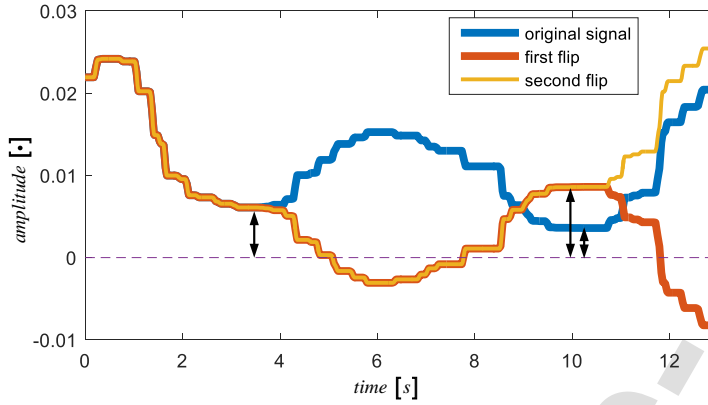
18

$$VP_{k,m}(s) = VP_{k,m}(s(t)).$$ (24)

Fig. 8. Flipping of the signal, leading to $p_{k,m}(t)$. Estimation errors, β_{km}, at nodal lines are marked with arrows.
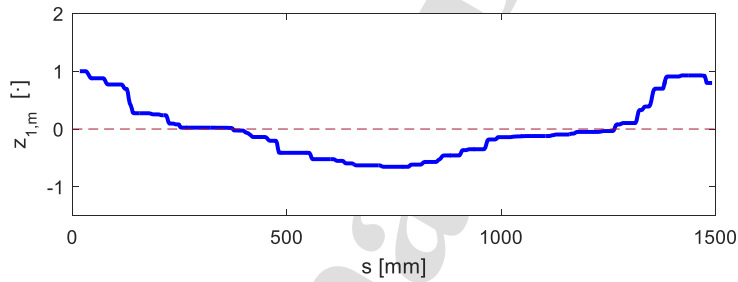

Fig. 9. Figure of improved VP estimation corresponding to the first bending mode.

3.3.3. SE size alternation

The previously extracted $VP_{k,m}$ is also influence by the SE size, m, used in the MMF. In Section 3.2, an SE of $m = 1024$ was chosen by trial and error, leading to the $VP_{k,1024}$ of the first three bending modes of the beam in Fig. 10(a). To investigate the impact of the chosen value, two additional filter settings were considered, with the results for $m = 128$ and $m = 16$ shown in Fig. 10(b) and Fig. 10(c) respectively.

19

The $VP_{k,1024}$ in Fig. 10 has clearly defined minima and maxima. As shown in Fig. 10(a), when m is too large, the noise reduction becomes excessive, which seriously damages the extracted mode shape and turns it into a stepping pattern. As m becomes smaller, the extracted $VP_{k,m}$ shape become more continuous, also the signal shows an increase in noise, which makes an extraction of the nodal lines with the described approach from Section 0 much more complicated. To overcome this issue, a mixture of different filter settings will be used in the final approach to extract the VP. A large SE size of $m = 1024$ is used to identify the local extrema, while a smaller SE size of $m = 128$ is applied to obtain the final, somewhat smoother, shapes.
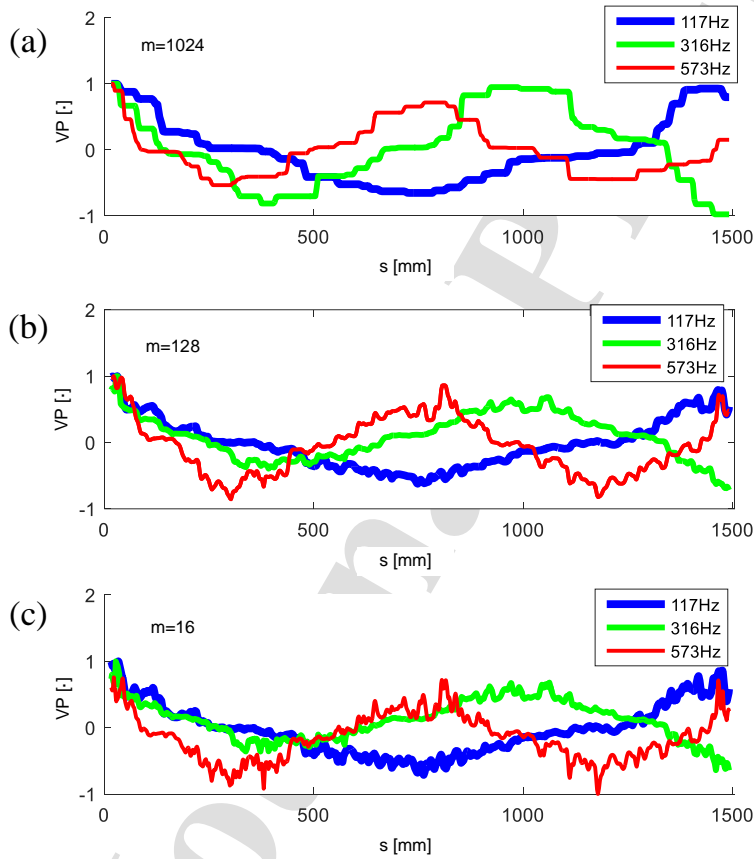

Fig. 10 First three extracted VP estimations with (a) SE size $m = 1{,}024$, (b) SE size $m = 128$, and (c) SE size $m = 16$.

20

It is worth noting that the length of structural elements is calculated by using sampling points. The number of sampling points included in the test results is related to the sampling frequency, the motion time of the Hexbug robot and other working conditions. Therefore, it was impossible to determine the length of structural elements according to prior knowledge, and empirical selection is needed according to the actual situation. The length of structural elements has to be optimized adaptively by using multiple iterations.
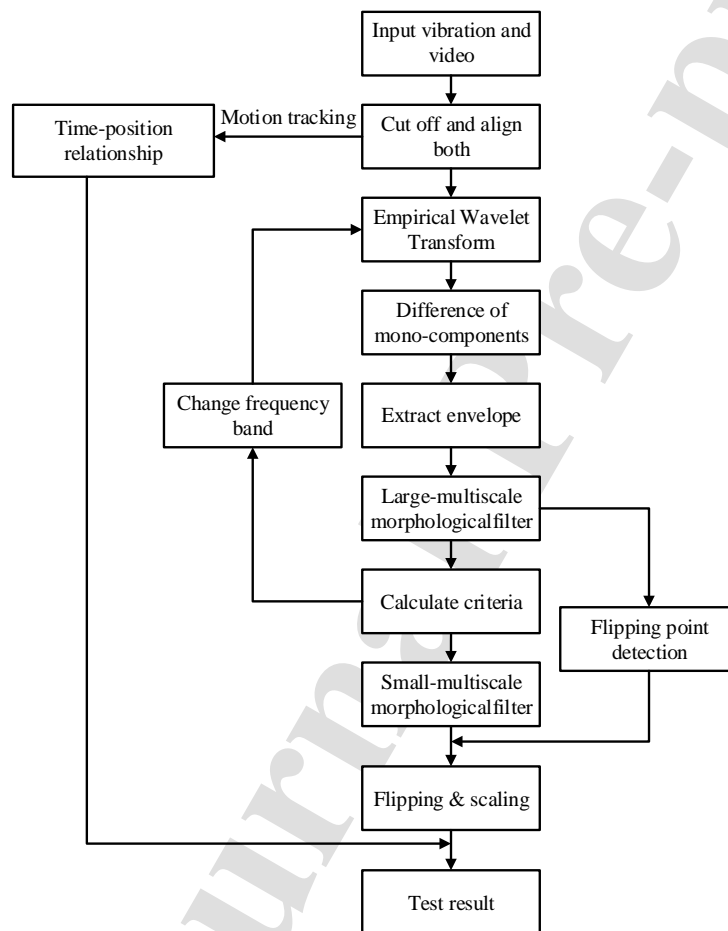

Fig. 11. Flowchart of the proposed data processing method.

21

3.4. Final approach

The final approach to extract the VP of several excited resonance frequencies from a single measurement with a roving excitation system is summarised in Fig. 11. Due to the unknown forcing function and variable excitation location, several post processing steps are needed to obtain the final results.

Fig. 12 shows a comparison of the obtained VP for the first three modes of the free-free beam with the experimental mode shapes obtained from the impact hammer test. It can be observed that the proposed approach with a roving robotic exciter, a single point measurement, and the newly developed data analysis technique allows to capture the first three VPs of the free-free beam reasonably accurately, confirming the feasibility of the introduced technique.
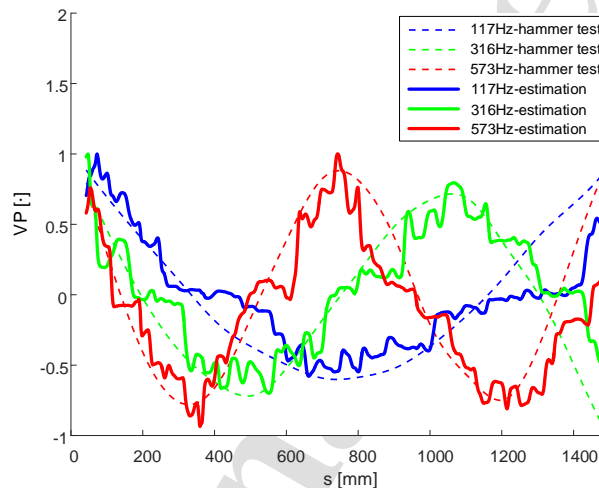

Fig. 12. Plots of the final extracted results of the first three VPs from single test, corresponding mode shapes are plotted in dashed lines.

4. Repeatability and Extraction Quality of VP

Due to the continuous roving random excitation, the acquired vibration signal can differ significantly between different measurements, raising the question of repeatability of the VP extraction technique. In order to quantify the similarity of the extracted $VP_{k,m}$ to the measured mode

22

shape from the hammer test (Section 2), the Pearson's correlation coefficient pcc and root mean square rms can be used

$$pcc_{l_1,l_2} = \left| \frac{\sum_{t=0}^{T}\left(l_1(t)-m_{l_1}\right)\left(l_2(t)-m_{l_2}\right)}{\sqrt{\sum_{t=0}^{T}\left(l_1(t)-m_{l_1}\right)^2}\sqrt{\sum_{t=0}^{T}\left(l_2(t)-m_{l_2}\right)^2}} \right| . \, , \tag{25}$$

$$rms_{l_1,l_2} = \sqrt{\sum_{t=0}^{T}\left(l_1(t)-l_2(t)\right)^2} \, , \tag{26}$$

where $l_1(t)$ and $l_2(t)$ are the two signals being compared to each other and $m_{l_1} = \frac{1}{T}\sum_{t=0}^{T}l_1(t)$ and $m_{l_2} = \frac{1}{T}\sum_{t=0}^{T}l_2(t)$. If $l_1(t)$ and $l_2(t)$ are similar, the rms value will approach 0 and the pcc will tend towards 1. Although the shape of the vibration shape is only determined by the inherent characteristics of the structure. However, due to the randomness of the excitation, there may be significant differences in the amplitude of the collected vibration modes, and it has a greater impact on the comparison of the vibration mode similarity. The measured mode shapes were consequently normalized to unity to be consistent with the corresponding extracted VP, and it was ensured that their initial value at $s = 0$ was positive, to ensure the correct phasing of the shapes.

A total of thirty roving excitation measurements on the free-free beam were conducted and the VP of the first three modes was extracted with the approach described previously. For each extracted VP the pcc and rms values with regards to the measured mode shapes from the hammer test was computed and their mean values $\overline{pcc_{VP_{k,m},MS_k}}$ and $\overline{rms_{VP_{k,m},MS_k}}$ with their standard deviations for each mode obtained. It can be seen in Table 1 that the average pcc values for all modes are above 0.9 and the rms values are around 0.2, with both having very small standard deviation. This indicates (i) that in general the extracted VP are close to the measured mode shapes from the hammer test, regardless of the remaining noise in the VP in Fig. 12; (ii) the extracted VPs from the thirty tests are all very similar to each other, leading to a very small standard deviation; and (iii) the first three modes can all be extracted with a similar level of accuracy.

Instead of analysing each data set individually to obtain a VP, the available data can also be used to create an averaged envelope function $\overline{A_k}$ from the processed individual envelopes, A_k, to estimate

22 / 31

23

a single VP of the system. Comparing this averaged envelope $\overline{A_k}$ in Fig. 13 (a) to a typical individual A_k in Fig. 6(a) a much better-defined signal shape is apparent even though some noise remains. The extracted VP from this averaged $\overline{A_k}$ is shown in Fig. 13(b) leading to a further improved match with the measured mode shapes, when compared to the results of an individual VP extraction from Fig. 12.

Table 1. Mean and standard deviation of the pcc and rms values for the 1$^{\text{st}}$ three modes (N = 30 tests).

30 tests	1$^{\text{st}}$ mode	2$^{\text{nd}}$ mode	3$^{\text{rd}}$ mode	average
pcc value	0.9051±0.0518	0.9081±0.0533	0.9084±0.0518	0.9072±0.0358
rms value	0.2138±0.0586	0.2140±0.0504	0.2565±0.0499	0.2281±0.0350

This implies that averaging multiple testing results can further improve the final VP. To better understand the impact of the envelop averaging, a series of VP has been computed, based on an increasing number of averages. Individual pcc and rms values where then computed to compare them to the hammer test results. Fig. 14 shows the pcc and rms values, averaged over the three modes, for different numbers of included measurements. For the current application about 10 to 15 measurements are required to achieve convergence with the measured mode shapes, suggesting that the proposed approach from Section 3 could be further improved by including averaging.

5. Cantilever beam validation

To investigate the applicability of the proposed method to a wider range of problems, the C-section from Fig. 2 was clamped on one side to form a cantilever beam (free length of 1,220 mm) as shown in Fig. 15. A single accelerometer was attached to the underside of the beam towards the free end (exit) and the roving exciter was placed on the beam at the back end of the clamp, as shown in the Fig. 15. The vibration signals were recorded as soon as the robot entered the cantilevered section.
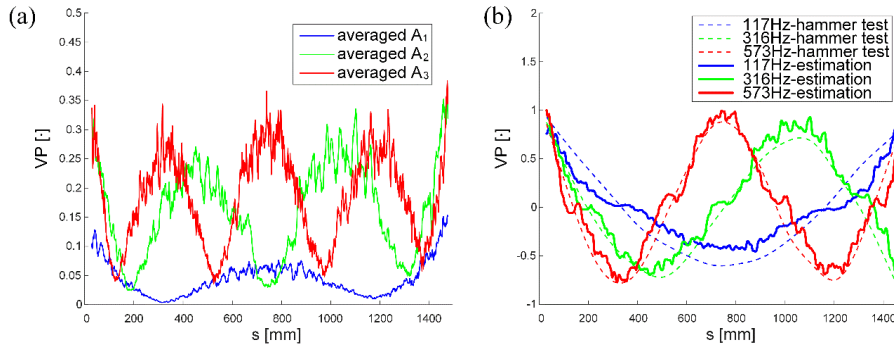
24

Fig. 13. Averaging over 30 measurements, (a) the first three $\overline{A_k}$ and (b) the corresponding extracted VP along with mode shapes in dashed lines.
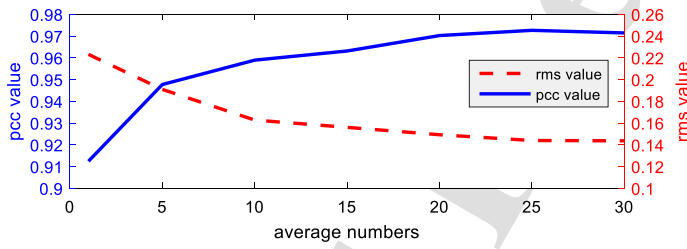

Fig. 14. The mean value of the two criteria for the first three VP estimation averaged over different number of multiple tests indicate convergence after about 10 to 15 samples.
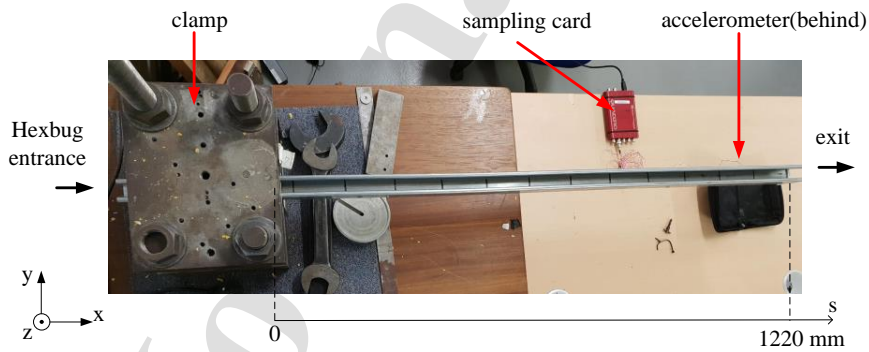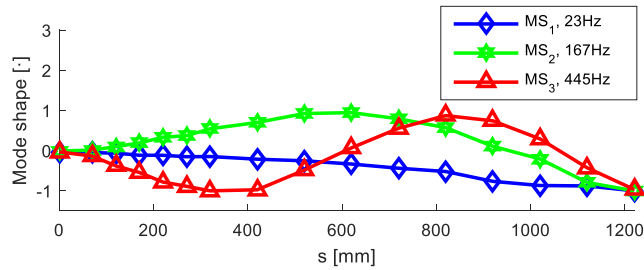

Fig. 15. Cantilever beam set up

25

Fig. 15. First three mode shapes of the cantilever beam in vertical direction.

An example of the roving exciter response signal can be seen in Fig. 16(a) along with its frequency spectrum in (b). Many resonances are being excited by the modified Hexbug, indicating that the little robot once more can introduce energy over a wide frequency band to the lightly damped system. The developed method was used to extract the first three VPs from the signal in Fig. 16(a), leading to the shapes in Fig. 17(a). A reasonably good agreement was achieved, also some inconsistencies in the amplitude was present.
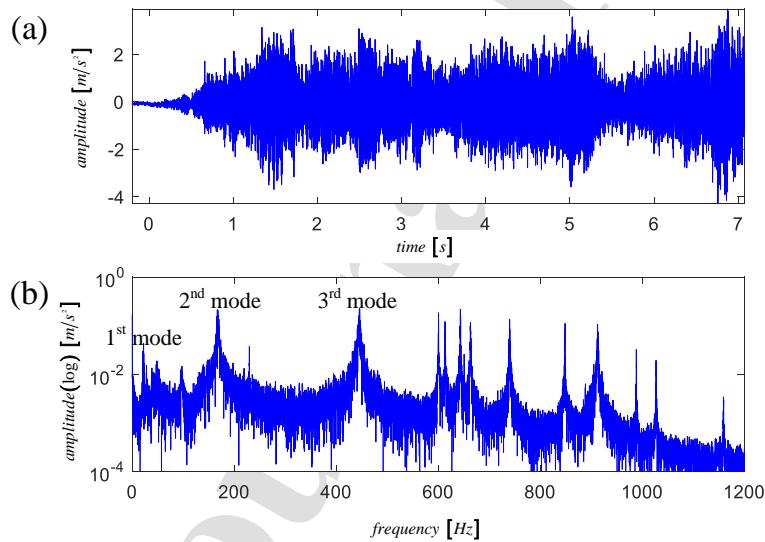

Fig. 16. Cantilever beam response, (a) time history and (b) frequency spectrum.
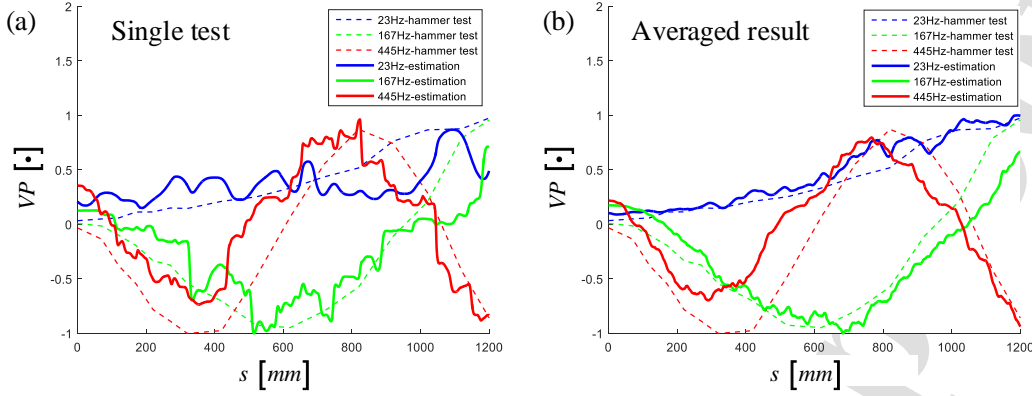
Fig. 17. First three VPs of the cantilever beam, (a) single signal from data in Fig.18 and (b) average result over 15 measurements.

Table 2. Similarity criteria for the averaged VPs of the cantilever beam

Average result	1st mode	2nd mode	3rd mode	average
pcc value	0.9668	0.9021	0.9590	0.9426
rms value	0.1049	0.2499	0.2360	0.1969

To minimise these effects, averaging of 15 envelopes, as proposed in Section 4, was used, leading to a significantly better agreement with the measured mode shapes in Fig. 17(b). The corresponding similarity criteria between the averaged result and the measured mode shapes are given in Table 2. The two criterion values indicate that the proposed method extracts the first three VPs of the cantilever beam with acceptable accuracy, highlighting the applicability of the technique for systems with different boundary conditions.

6. Discussion

A novel VP extraction method for one-dimensional structure such as pipes and beam sections has been presented with unknown input and a single output, based on a roving continuous random excitation.

27

The main benefit of the proposed method is that it provides a relatively simple way to obtain acceptably accurate VP from a structure. Compared with multi-point simultaneous vibration measurements, this method only requires a single measurement location, combined with the roving random continuous exciter, which alleviates the often problematic access to structures with the measurement equipment. The proposed method has the potential to help with the measurement of interior components or difficult to access pipework, as long as the exciter can be placed on it somewhere, and a single location is accessible for the measurement. The second benefit is that it could split the frequency bands automatically and transform the complex signal into VPs easily because of the modification based on EWT.

The currently used exciter system, based on a slightly modified Hexbug Nano v2© introduces enough forcing to excite a wide range of resonance frequencies, but it leads to a rather unpredictable motion, which diminishes the above advantage somewhat. To overcome this issue a slightly more advanced exciter could be used in the future that ensures linear motion along the pipe or channel. The system in its current form has been developed for 1D motion along a pipe or open beam section, but a very similar approach could be developed for 2D structures (e.g., panels), if the exciter can be located accurately.

A series of assumption has been made during the development of the analysis technique for the roving random excitation, including (i) the structure has a linear dynamic response; (ii) although $F(t)$ is unknown and random, it is assumed to be a stationary process; (iii) the resonance frequencies of the structure are well separated in the frequency domain; and (iv) the sampling frequency is high enough to ensure that $\omega_j \delta$ is very small. Fortunately, the acceptability of these assumptions has been confirmed by the good agreement between the measured mode shapes from the impact hammer test, and the extracted VP results.

It was shown that both the frequency boundaries $\{\omega_i\}$ used in EWT and SE size m used for the MMF, can strongly impact the extracted VP shapes. The correct selection of these values is therefore of uttermost importance. To ensure an accurate extraction of the mono-components, f_k, two indexes have been defined which allow using optimisation techniques to reduce errors at the nodal locations. The parameter, m, which is used in the MMF processing influences the balance between noise

28

reduction in the signal, and the shape preservation, and as such its correct selection can have a major impact on the quality of the extracted VP. Its influence on the result is linked to other parameters as well, including the sampling and resonance frequency. A trial-and-error approach is recommended to overcome this issue. It should be noticed that, for a different structure, these parameters may be different.

The introduced vibration excitation system introduces randomness and noise into the VP analysis procedure which makes the analysis very challenging. Quite a bit of uncertainty is present in the actual forcing function, $F(t)$, such as the additional impact force generated when the robot was placed on the structure and dropped from the system. Great care needs to be taken to minimise these effects, or if that is not possible, removing the impacted parts of the data set may need to be considered. In addition, the data processing itself is introducing additional challenges, where in particular the multi-scale morphological filter leads to non-zero values close to the nodal line. An approach was presented to compensate for these effects, but some distortion in the VP shapes remains.

7. Conclusion

A novel vibration pattern (VP) measurement method with unknown input and a single output, particularly suited for pipes and other long slender structures, has been presented. The approach is based on a small robotic device that excites the structures as it moves along, a single measurement location to acquire the vibration response, and an advanced data post-processing technique to extract the VPs from the measured signal.

An experimental setup was developed, demonstrating the capability of a slightly modified Hexbug Nano v2 © toy robot to excite a large range of frequencies in a lightly damped slender C-section beam. High-quality response data was acquired for a free-free and cantilevered setup, highlighting the strong modulation of the response by the excited mode shapes.

An advanced data post-processing routine was introduced, combining Empirical Wavelet Transform and MMF, to analyse the single output response from the roving excitation source. Several challenges, including the influence of the unknown forcing function, the separation of the different response modes, the variable position of the excitation system, and the extraction of the response envelopes and their reassembly, were addressed to allow the extraction of the vibration patterns.

The method we propose uses a simple and cheap experimental setup to measure accurately the VPs of long slender structures and verified the feasibility of this method. The method developed could potentially replace or combined with other conventionally applied measurement methods, such as direct inspections of pipes using robotic devices or ultrasound sensor networks which are more complex, time-consuming, require more space or expensive. Also, refining the method proposed here further, by decreasing the size of the exciters, with the aim to study larger, more complex structures and machines which cannot easily assembled is envisaged with foreseeable interest to a range of applications and research fields.

Acknowledgement

References

[1] D. J. Ewins, Modal Testing, Theory. "Practice and Application, second ed." *Research Studies Press Ltd*, UK, 2000.

[2] M. H. Richardson, Is it a Mode Shape, or an Operating Deflection Shape? Sound & Vibration 1 (1997) 1–11.

[3] B. J. Schwarz, M. H. Richardson. "Introduction to operating deflection shapes." *CSI Reliability Week* 10 (1999) 121-126.

[4] C. Ratcliffe, D. Heider, R. Crane, C. Krauthauser, M. K. Yoon, J. W. G. Jr. "Investigation into the use of low cost MEMS accelerometers for vibration based damage detection." *Composite Structures* 82 (2008) 61-70.

[5] M. K. Yoon, D. Heider, J. W. Gillespie, C. P. Ratcliffe, R. M. Crane. "Local Damage Detection with the Global Fitting Method Using Operating Deflection Shape Data." *Journal of Nondestructive Evaluation* 29 (2010) 25-37.

[6] C. Zhang, Y. Liu, F. Wan, B. Chen, B. Hu. "Adaptive filtering enhanced windowed correlated kurtosis for multiple faults diagnosis of locomotive bearings." *ISA Transactions* 101 (2020) 421-429.

[7] A. Hu, J. Zhao, X. Ling. "Output-only modal analysis of wind turbine tower based on vibration response under emergency stop." *ISA transactions*, 80 (2018) 411-426.

[8] A. Hafiz, T. Schumacher. "Effects of elastic supports and flexural cracking on low and high order modal properties of a reinforced concrete girder." *Engineering Structures* 178 (2019) 573-585.

[9] G. Ebi, "Operating deflection shape analysis - A powerful tool to increase plant reliability." *Hydrocarbon Processing* 80 (2001) 59-63.

[10] S. J. Rothberg, M. S. Allen, P. Castellini, D. D. Maio. "An international review of laser Doppler vibrometry: Making light work of vibration measurement." *Optics & Lasers in Engineering* 99.dec. (2016) 11-22.

[11] A. B. Stanbridge, D. J. Ewins, "A review of 10 years of continuous-scan LDV developments." *Proceedings of International Conference on Noise and Vibration Engineering ISMA2006.*" 1–8 (2006) 3165–3179.

30

[12] S. P. Yam, Z. Brodzeli, S. A. Wade, C. M. Rollinson, G. W. Baxter, and S. F. Collins. "Use of first-order diffraction wavelengths corresponding to dual-grating periodicities in a single fibre Bragg grating for simultaneous temperature and strain measurement." 2009 *Meas. Sci. Technol.* 20 034008.

[13] A. A. P. Pohl, R. A. Oliveira, R. E. Da Silva, C. A. F. Marques, P. T. Neves Jr., K. Cook, J. Canning, and R. N. Nogueira. "Advances and new applications using the acousto-optic effect in optical fibers." *Photonic Sens* 3, 1–25 (2013).

[14] S. W. Khoo, S. Karuppanan, C. S. Tan. "A Review of Surface Deformation and Strain Measurement Using Two-Dimensional Digital Image Correlation." *Metrology and Measurement Systems* 23 (2016) 461-480.

[15] F. Oudah, R. El-Hacha. "Damage and deformation assessment of earthquake-resistant RC slotted beam-column connections using digital image correlation technique." *Engineering Structures* 215 (2020) 110442.

[16] J. D. Maynard, E. G. Williams, and Y. Lee. "Nearfield acoustic holography: I. Theory of generalized holography and the development of NAH." *The Journal of the Acoustical Society of America* 78 (1985) 1395.

[17] S. F. Wu. "Hybrid near-field acoustic holography." *The Journal of the Acoustical Society of America* 115, 207 (2004).

[18] X. J. Dai, X. X. Shao, Z. C. Geng, F. J. Yang. "Vibration measurement based on electronic speckle pattern interferometry and radial basis function." *Optics Communications* 355 (2015) 33-43.

[19] M. Lu, S. Wang, L. Aulbach, A. W. Koch. "Simultaneous displacement and slope measurement in electronic speckle pattern interferometry using adjustable aperture multiplexing." *Applied Optics* 55 (2016) 5868.

[20] C. Collette, A. Preumont. "Laser measurement of torsional vibrations/longitudinal creepage of a railway wheel set on a scaled test bench." *Optics & Lasers in Engineering* 47 (2007) 385-389.

[21] C. W. Schwingshackl, L. Massei, C. Zang. "A constant scanning LDV technique for cylindrical structures: Simulation and measurement." *Mechanical Systems & Signal Processing* 24 (2010) 394-405.

[22] L. E. Olson, A. Abrego, D. Barrows. "Blade Deflection Measurements of a Full-Scale UH-60A Rotor System." *American Helicopter Society Aeromechanics Specialist Conference, San Francisco, CA* 2010.

[23] Z. Yao, L. Wang, Z. Xiang. "Damage detection by mode shape squares extracted from a passing vehicle." *Journal of Sound & Vibration* 331 (2012) 291-307.

[24] Y. Oshima, K. Yamamoto, and K. Sugiura. "Damage assessment of a bridge based on mode shapes estimated by responses of passing vehicles." *Smart Structures & Systems* 13 (2014) 731-753.

[25] W. J. Palm. "Mechanical vibration." *Wiley & Sons* 4649 (2007) 1581.

[26] J. Gilles. "Empirical Wavelet Transform." *IEEE Transactions on Signal Processing* 61 (2013) 3999-4010.

[27] J. Zheng, H. Yang, S. Cheng. "Adaptive parameterless empirical wavelet transform based time-frequency analysis method and its application to rotor rubbing fault diagnosis." *Signal Processing* 130 (2017) 305-314.

[28] J. Pan, J. Chen, Y. Zi. "Data-driven mono-component feature identification via modified nonlocal means and MEWT for mechanical drivetrain fault diagnosis." *Mechanical Systems and Signal Processing* 80 (2016) 533-552.

[29] P. Maragos, W. Schafer. "Morphological filters—part I: Their set-theoretic analysis and relations to linear shift-invariant filters." *IEEE Transactions on ASSP* 35 (1987) 1153–1169.

[30] W. Jing, G. Xu, Q. Zhang, L. Lin. "Application of improved morphological filter to the extraction of impulsive attenuation signals." *Mechanical Systems & Signal Processing* 23 (2009) 236-245.

[31] N. G. Nikolaou, I. A. Antoniadis. "Application of morphological operators as envelope extractors for impulsive-type periodic signals." *Mechanical Systems & Signal Processing* 17 (2003) 1147-1162.

[32] Y. Li, M. J. Zuo, J. Lin, J. Liu. "Fault detection method for railway wheel flat using an adaptive multiscale morphological filter." *Mechanical Systems and Signal Processing* 84 (2017) 642-658.

31

[33] T. Gong, Y. Yuan, X. Yuan. " Application of optimized multiscale mathematical morphology for bearing fault diagnosis." *Measurement Science and Technology* 28 (2017) 045401.

[34] S. L. Hahn. "Hilbert Transform in Signal Processing." *Artech House Publish* (1996).

Declaration of interests

☒ The authors declare that they have no known competing financial interests or personal relationships that could have appeared to influence the work reported in this paper.

☐ The authors declare the following financial interests/personal relationships which may be considered as potential competing interests: